Journal of Solid State Chemistry 186 (2012) 165–170

Contents lists available at SciVerse ScienceDirect

Journal of Solid State Chemistry

journal homepage: www.elsevier.com/locate/jssc

Hydrothermal synthesis, crystal structures and photoluminescence properties of mixed europium–yttrium organic frameworks

Yinfeng Han [a,b], Lianshe Fu [c], Luís Mafra [a,*], Fa-Nian Shi [a,*]

[a] Department of Chemistry, CICECO, University of Aveiro, 3810-193 Aveiro, Portugal
[b] Department of Chemistry and Environmental Science, Taishan University, Taian 271021, China
[c] Department of Physics, CICECO, University of Aveiro, 3810-193 Aveiro, Portugal

ARTICLE INFO

Article history:
Received 25 September 2011
Received in revised form
29 November 2011
Accepted 4 December 2011
Available online 13 December 2011

Keywords:
Metal-organic framework
Mixed lanthanide
Light-emitter
Photoluminescence
Topology

ABSTRACT

Three mixed europium–yttrium organic frameworks: $Eu_{2-x}Y_x(Mel)(H_2O)_6$ (Mel=mellitic acid or benzene-1,2,3,4,5,6-hexacarboxylic acid, x=0.38 **1**, 0.74 **2**, and 0.86 **3**) have been synthesized and characterized. All the compounds contain a 3-D net with (4, 8)-flu topology. The study indicates that the photoluminescence properties are effectively affected by the different ratios of europium and yttrium ions, the quantum efficiency is increased and the Eu^{3+} lifetime becomes longer in these MOFs than those of the Eu analog.

1. Introduction

Metal-organic frameworks (MOFs) or porous coordination polymers (PCPs) have been under intense investigations due to diverse structural architectures and potential applications in gas storage, separation, catalysis and molecular recognition [1–9]. Over the decade years, many MOFs based on lanthanide (*Ln*) ions and aromatic polycarboxylates have been extensively studied [3,9–24]. The luminescent *Ln* organic frameworks are demonstrating a great potential as light sensors because they are becoming a class of light-emitting materials with good performance in single color light, high strength, high internal quantum efficiency and high stability [9–24]. Presently, several works focus on the doping *Ln* ions into nanoparticles to enhance their fluorescent intensities, albeit a number of reports have been reported regarding the incorporation of different *Ln* ions into MOFs [25–28]. If *Ln* ions are doped in MOFs, the fluorescent intensity will be improved and, consequently, the quantum efficiency will also be increased due to the elimination or decrease of concentration quenching effect. Zhang et al. reported nanoscale $Eu_{1-x}Tb_x$-MOFs as luminescent thin films with strong luminescent properties and efficient Tb^{3+}-to-Eu^{3+} energy transferability [29]. Williams et al. investigated the quantifying enhanced photoluminescence from just 0.1% doping of Eu into Tb carboxylate coordination polymers [30]. It is noticed that, in these mixed *Ln* MOFs, the *Ln* ions are all luminescent ions [11,29–31]. The luminescent properties of *Ln* MOFs can also be modified via introducing an inert *Ln* ion (ca. yttrium) into luminescent ions frameworks [13,32,33]. Mellitic acid (Mel), an organic ligand with six carboxylate groups, is able to form porous MOFs with high thermal stabilities and up to now, a series of MOFs based on Mel and metal ions have been synthesized [34–39]. In this work, Mel ligand that contains no hydrogen atom in its aromatic ring was chosen due to no hydrogen thermal vibration, which is clearly advantage for the *Ln* luminescence. In order to investigate luminescence properties upon incorporation of inert *Ln* ions into Mel-based MOFs, here we report a series of mixed europium–yttrium organic frameworks: $Eu_{2-x}Y_x$(Mel)$(H_2O)_6$ (x=0.38 **1**, 0.74 **2**, and 0.86 **3**). In addition, we also synthesized the analogs with singular Eu^{3+} or Y^{3+}: $Eu_2(Mel)(H_2O)_6$ **4** and $Y_2(Mel)(H_2O)_6$ **5** to allow the comparison of the luminescence properties with **1**, **2**, and **3.**

2. Experimental section

2.1. Materials and general methods

Chemicals were readily available from commercial sources and were used as received without further purifications: *Ln*(III) nitrate hydrates ($Ln(NO_3)_3 \cdot xH_2O$, *Ln*=Eu and Y; ≥99.9%, Sigma-Aldrich); Mel ($C_{12}H_6O_{12}$, ≧97%, Aldrich).

* Corresponding authors.
E-mail addresses: lmafra@ua.pt (L. Mafra), fshi@ua.pt (F.-N. Shi).

0022-4596/$ - see front matter © 2011 Elsevier Inc. All rights reserved.
doi:10.1016/j.jssc.2011.12.007

SEM was performed using a Hitachi Su-70 and energy dispersive analysis of X-rays spectroscopy (EDS) was carried out on a Bruker QUANTAX 400 instruments working at 15 kV. Samples were prepared by deposition on aluminum sample holders by carbon coating. FTIR spectra were collected from KBr pellets (Aldrich, 99%+, FTIR grade) with a Mattson 7000 FTIR spectrometer. Thermogravimetric analyses were carried out in air using a Shimadzu TGA-50, with a heating rate of 5 °C/min and a flow rate of 20 cm^3/min. Conventional powder X-ray diffraction data for the materials were collected at ambient temperature with an X'Pert MPD Philips diffractometer ($CuK\alpha_{1,2}$ X-radiation, $\lambda_1=1.540598$ Å and $\lambda_2=1.544426$ Å), equipped with an X'Celerator detector and a flatplate sample holder in a Bragg–Brentano para-focusing optics configuration (40 kV, 50 mA). Intensity data were collected by the step counting method (step 0.02°), in continuous mode, in the ca. $5 \leqq 2\theta \leqq 50°$ range.

The photoluminescence spectra were recorded at RT with a modular double grating excitation spectrofluorimeter with a TRIAX 320 emission monochromator (Fluorolog-3, Horiba Scientific) coupled to a R928 Hamamatsu photomultiplier, using a front face acquisition mode. The excitation source was a 450 W Xe arc lamp. The emission spectra were corrected for detection and optical spectral response of the spectrofluorimeter and the excitation spectra were corrected for the spectral distribution of the lamp intensity using a photodiode reference detector. The emission decay curves were measured with the setup described for the luminescence spectra using a pulsed Xe–Hg lamp (6 ms pulse at half width and 20–30 ms tail).

2.2. Syntheses

2.2.1. $Eu_{1.62}Y_{0.38}(Mel)(H_2O)_6$ **1**

A mixture of Mel (0.342 g, 1.00 mmol), $Eu(NO_3)_3 \cdot 6H_2O$ (0.357 g, 0.80 mmol) and $Y(NO_3)_3 \cdot 6H_2O$ (0.076 g, 0.20 mmol) was stirred in distilled water (15 ml) at room temperature (RT) for 30 min, then sealed in a Teflon-lined stainless steel autoclave (40 ml) and heated at 150 °C for 1 day under autogenous pressure. After cooling to RT, the colorless crystals were washed three times with distilled water (3×10 ml) and air dried at ambient temperature.

2.2.2. $Eu_{1.26}Y_{0.74}(Mel)(H_2O)_6$ **2**

The synthesis procedure is similar to compound **1**, only $Eu(NO_3)_3 \cdot 6H_2O$ (0.313 g, 0.70 mmol) and $Y(NO_3)_3 \cdot 6H_2O$ (0.115 g, 0.30 mmol) substituted the previous amounts of *Ln* compounds.

2.2.3. $Eu_{1.14}Y_{0.86}(Mel)(H_2O)_6$ **3**

The synthesis procedure is similar to compound **1**, only $Eu(NO_3)_3 \cdot 6H_2O$ (0.268 g, 0.60 mmol) and $Y(NO_3)_3 \cdot 6H_2O$ (0.153 g, 0.40 mmol) substituted the previous amounts of *Ln* compounds.

2.3. Crystallographic data collection and structure

Complete single-crystal data of **1**–**5** were collected at 150(2) K on a Bruker X8 Kappa APEX II charge-coupled device (CCD) area-detector diffractometer ($MoK\alpha$ graphite monochromated radiation, $\lambda=0.7107$ Å) controlled by the APEX2 software package [40] and equipped with an Oxford Cryosystems Series 700 cryostream monitored remotely by using the software interface Cryopad [41]. Images were processed using the software package SAINT+ [42]. Absorption corrections were applied by the multiscan semiempirical method implemented in SADABS [43]. The structure was solved by direct method using SHELXS-97 [44,45] and refined using SHELXL-97 [44]. All non-hydrogen atoms were successfully refined with anisotropic displacement parameters. The quantity of Eu and Y atoms in the structures of **1**–**3** was well treated with substitutional disorder by using EXYZ, EADP and PART instructions. Hydrogen atoms bound to carbon were located at their idealized positions by employing the HFIX 43 instruction in SHELXL-97 and included in subsequent refinement cycles in riding motion approximation with isotropic thermal displacement parameters (U_{iso}) fixed at $1.2U_{eq}$ of the carbon atom to which they were attached. The hydrogen atoms associated with water molecules were visible in the last difference Fourier maps synthesis. These atoms have been included in the final structural models with the O–H distances restrained to 0.85(1) Å, in order to ensure a chemically reasonable geometry for these moieties, and with U_{iso} fixed at $1.2U_{eq}$ of the parent oxygen atoms. The detailed crystallographic data and structural refinement parameters have been summarized in Table 1.

3. Results and discussion

3.1. SEM and PXRD

All the compounds were prepared by hydrothermal synthesis. The scanning electron microscopy (SEM) image (Fig. 1) shows an almost homogeneous size distribution of the particles and similar crystal habits in all compounds. The EDS analysis showed that the

Table 1
Crystallographic data and structural refinements for **1**–**5**.

	1	**2**	**3**	**4**	**5**
Empirical formula	$C_6H_6O_9Eu_{0.81}Y_{0.19}$	$C_6H_6O_9Eu_{0.63}Y_{0.37}$	$C_6H_6O_9Eu_{0.57}Y_{0.43}$	$C_6H_6O_9Eu$	$C_6H_6O_9Y$
Formula weight	361.93	351.05	347.27	374.07	351.05
Crystal system	Orthorhombic	Orthorhombic	Orthorhombic	Orthorhombic	Orthorhombic
Space group	*Pnnm*	*Pnnm*	*Pnnm*	*Pnnm*	*Pnnm*
a (Å)	13.3917(16)	13.3666(14)	13.3827(8)	13.3963(6)	13.3270(10)
b (Å)	6.6018(9)	6.5878(6)	6.5921(4)	6.6071(3)	6.5394(4)
c (Å)	10.1228(12)	10.0968(14)	10.1230(10)	10.1307(4)	10.0679(6)
Volume (Å^3)	894.95(19)	889.09(17)	893.05(12) Å^3	896.68(7)	877.42(10)
Z	4	4	4	4	4
D_{calc} (g cm^{-3})	2.686	2.623	2.583	2.771	2.354
R(int)	0.0537	0.0476	0.0266	0.0498	0.0143
μ (mm^{-1})	6.952	6.912	6.852 mm−1	7.033	6.686
F (0 0 0)	690	673	667	708	612
Data/restraints/parameters	1040/4/84	835/4/54	1424/4/97	1441/3/82	1006/3/82
GOF on F^2	1.046	1.079	1.086	1.033	1.108
$R_1[I>2\sigma(I)]$[a]	0.0296	0.0237	0.0195	0.0285	0.0211
$wR_2[I>2\sigma(I)]$[a]	0.0588	0.0492	0.0381	0.0486	0.0512
Larg. diff. peak & hole, e/Å^{-3}	0.836 and −1.725	0.472 and −0.655	0.553 and −0.694	1.156 and −1.355	0.476 and −0.523

compositions of Eu:Y=9:1 for (**1**), Eu:Y=7:3 for (**2**) and Eu:Y=6:4 for (**3**) were roughly in agreement with the molecular formula of (**1**), (**2**) and (**3**) that were derived from the single crystal structural data. The powder XRD patterns obtained for the as-synthesized compounds are shown in Fig. 2 and reveal that the materials are crystalline, pure and crystallize in the same structure as indicated by the single crystal data. All 2θ peaks are consistent with the corresponding simulated ones.

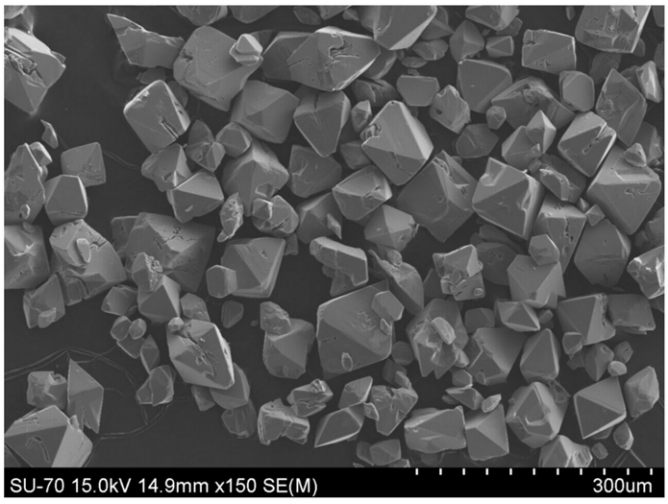

Fig. 1. SEM image of **1**.

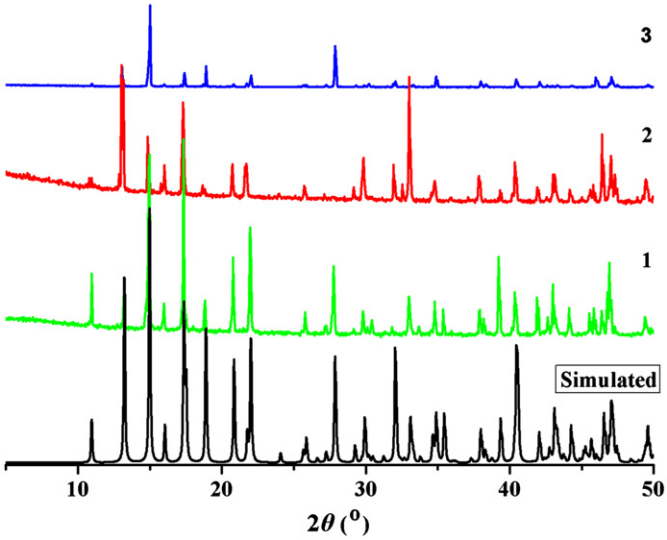

Fig. 2. XRD patterns of **1**, **2**, and **3**.

3.2. Structure

Single-crystal X-ray diffraction analysis reveals that **1**, **2** and **3** are isostructural crystallizing in orthorhombic space group *Pnnm*, structurally identical to the single *Ln* analogs, which were published elsewhere [37–39], thus, only the structure of **1** is described here.

In compound **1**, each *Ln* ion is coordinated by nine oxygen atoms from carboxyl groups and water molecules. All Mel groups are deprotonted and coordinated to eight *Ln* ions via two different coordination modes of carboxyl groups: one is bridging bidentate carboxyl groups and the other displays chelating bidentate coordination mode (Fig. 3). The *Ln*–O bond lengths range from 2.308(6) to 2.568(4) Å, which are longer than the Y–O bond lengths (2.277(2) to 2.550(2) Å) and shorter than the Eu–O bond lengths (2.324(4) to 2.577(3) Å), which indicate the incorporation of Eu^{3+} and Y^{3+} ions in compound **1**.

The structural feature of ligands and coordination modes of metal ion/clusters are two essential factors for investigating the topology of MOFs. In compound **1**, Mel anions act as 8-connected nodes to connect eight *Ln* ions. Each *Ln* ion can be considered as 4-connected nodes linked by four 8-coordinated Mel ions to form a (4, 8)-flu net (Fig. 4).

3.3. Thermal properties

TGA curves for compounds **1**–**3** in Fig. 5 displays similar thermal behaviors, thus only **1** is depicted in detail. Compound **1** shows three steps of weight losses (Fig. 5). The first weight loss of 4.72% is in agreement with the calculated value of the removal of a coordinated water molecule (4.98%) from 140 °C to 160 °C. The second step corresponds to the complete loss of the other two coordinated water molecules from 185 °C to 216 °C (observed value: 14.24%; calculated value: 14.94%). Above 400 °C, Mel species start to be decomposed, and the final residue of 46.47% is consistent with Eu and Y oxides (calculated: 45.30%).

3.4. Photoluminescence studies

1, **2** and **3** show the similar excitation profiles. Fig. 6 is the excitation spectrum of **3** measured at RT while monitoring the

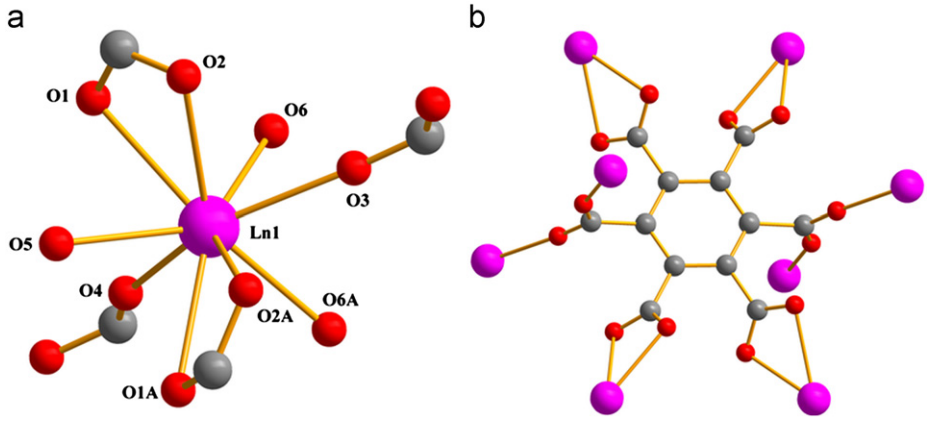

Fig. 3. (a) The coordination environment of *Ln* and (b) the coordination environment of Mel. Pink ball: Lanthanide atom; red ball: Oxygen atom; gray ball: Carbon atom. (For interpretation of the references to color in this figure legend, the reader is referred to the web version of this article.)

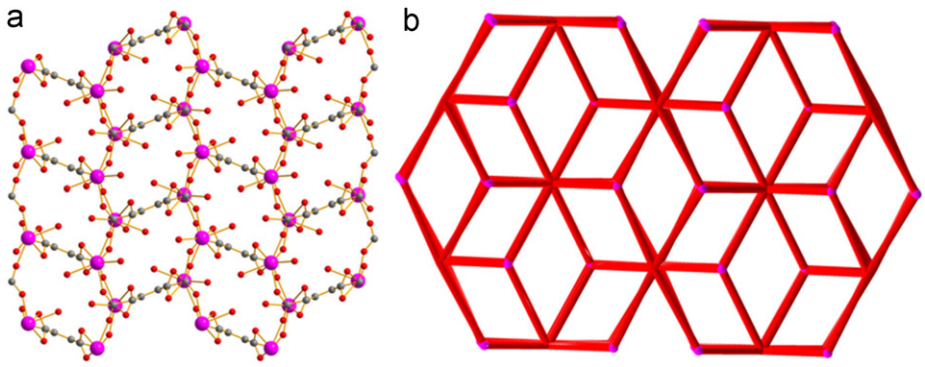

Fig. 4. (a) 3D network of **1** and (b) the topology structure of **1**. Pink ball: Lanthanide atom; red ball: Oxygen atom; gray ball: Carbon atom. (For interpretation of the references to color in this figure legend, the reader is referred to the web version of this article.)

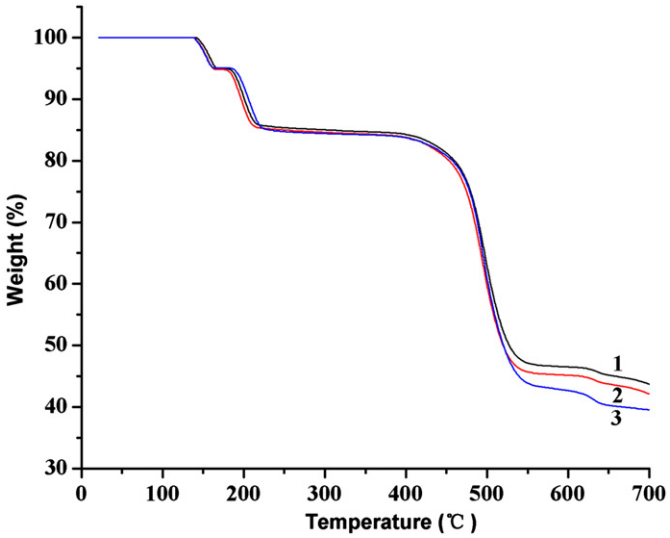

Fig. 5. TGA curves of **1**, **2**, and **3**.

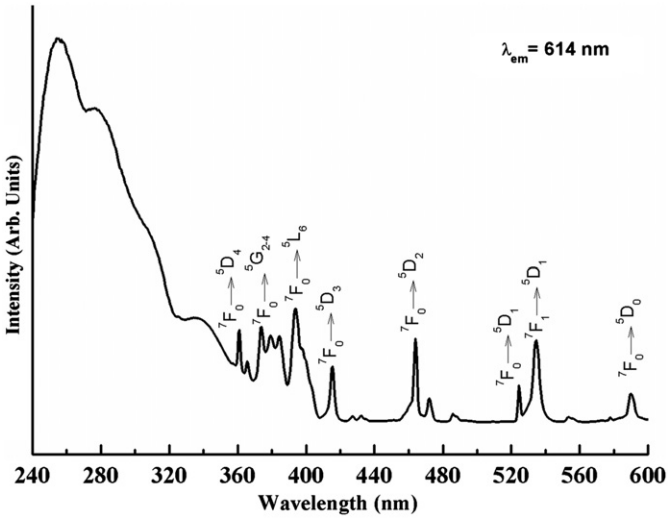

Fig. 6. Excitation spectrum of **3**.

Eu^{3+} emissions at 614 nm. The excitation spectrum exhibits a broad band between 240 and 360 nm with a maximum intensity at around 250 nm attributed to electronic transitions from the ground state level (π) S_0 to the excited level (π^*) S_1 of the organic ligand Mel. The sharp peaks observed in the 360–590 nm range

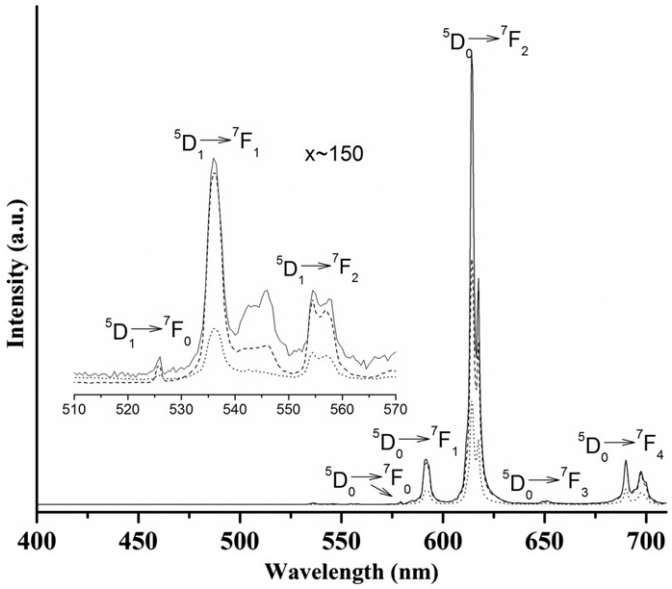

Fig. 7. Emission spectra of **3** excited at 250 nm (solid line), 300 nm (broken line) and 360 nm (dotted line), respectively. Inset: the enlarged part for the wavelength range between 510 and 570 nm.

result from the intra *f–f* transitions of the Eu^{3+} ions, which are characteristic of absorption lines of Eu^{3+} ions and their transition assignments are also indicated in the spectrum. Compared to the ligand absorption, the Eu^{3+} *f–f* transitions display the weak intensities, indicating that a sensitization of Eu^{3+} luminescence is mainly through an indirect energy transfer process from organic ligand to Eu^{3+} ions.

The emission spectra of **3** were investigated under different excitation wavelengths. All the spectra are composed of strong emission lines ascribed to transitions from $^5D_0 \rightarrow {}^7F_J$ (J=0–4), with the $^5D_0 \rightarrow {}^7F_2$ emission as the dominant band. In addition, the samples also show very weak emissions from $^5D_1 \rightarrow {}^7F_J$ (J=0–2) (Fig. 7, inset). No emission arising from the ligand triplet levels could be detected, suggesting an efficient energy transfer from the ligand Mel to Eu^{3+} ions.

Fig. 8 displays the emission features for **1**, **2** and **3** excited at 250 nm. All the spectra show the similar emission bands. The $^5D_0 \rightarrow {}^7F_2$ transition is a typical electric dipole transition and strongly varies with the local symmetry of Eu^{3+} ions, while the $^5D_0 \rightarrow {}^7F_1$ transition corresponds to a parity-allowed magnetic dipole transition, which is practically independent of the host material. Therefore, the intensity ratio of $^5D_0 \rightarrow {}^7F_2$ to $^5D_0 \rightarrow {}^7F_1$ (R) is sensitive to the symmetry around Eu^{3+} ions and gives valuable

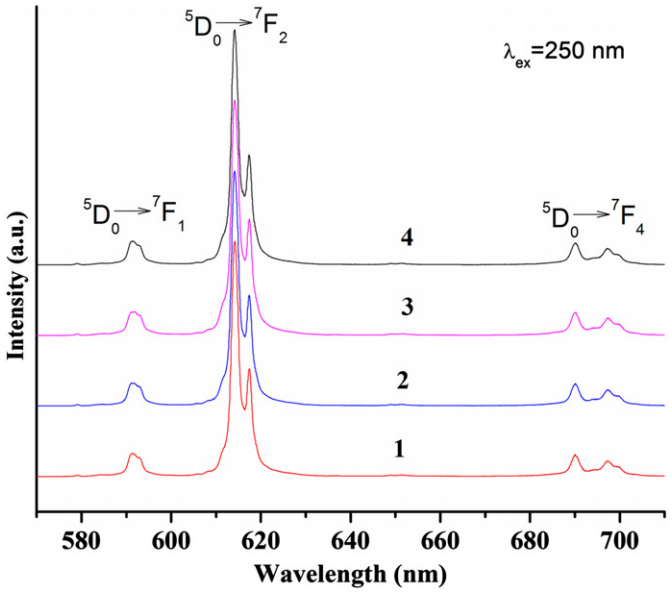

Fig. 8. Emission spectra for **1**, **2**, **3** and **4** excited at 250 nm.

Table 2
Experimental (k_{exp}) and calculated radiative (k_r) and nonradiative (k_{nr}) $^5D_0$ decay rates (m s^{-1}), decay time (τ, ms), quantum efficiency (q) and number of water molecules coordinated to Eu^{3+} ions (n_w).

Compound	τ (ms)	k_{exp} (m s^{-1})	k_r (m s^{-1})	k_{nr} (m s^{-1})	q (%)	$n_w/\pm 0.1$
1	0.304	3.289	0.576	2.713	17.5	2.7
2	0.317	3.155	0.591	2.564	18.7	2.5
3	0.327	3.058	0.590	2.468	19.3	2.4
4	0.304	3.289	0.558	2.731	17.0	2.7

information about environment change [46]. When the R value is higher, the Eu^{3+} ion occupies a site of lower symmetry without inversion center (more asymmetric local environment). In order to investigate the effect of Y^{3+} ions on the local symmetry of Eu^{3+} ions, the spectral deconvolutions were carried out. For the MOFs, with Eu: **4** and Eu/Y MOFs: **1**, **2** and **3**, the R values are 8.5, 8.7, 8.9 and 8.9, respectively. This indicates that when more Y^{3+} ions were mixed, a more asymmetric environment occupied by Eu^{3+} ions.

The luminescence decay curves of Eu^{3+} related to the $^5D_0 \rightarrow {}^7F_2$ emission were measured. All the decay curves for both Eu and Eu/Y MOFs are mono-exponential, confirming that all the Eu^{3+} ions lie in the same average environment. The luminescence lifetimes were listed in Table 2.

In order to further discuss luminescence features, the quantum efficiency (q) and the number of water molecules (n_w) coordinated to the Eu^{3+} ions were calculated according to the literatures [47,48], and the results are also reported in Table 2.

From Table 2, it can be clearly seen that when more Y^{3+} ions were incorporated, the Eu^{3+} ions lifetime increases, from 0.304 ms to 0.327 ms; the quantum efficiency also increases. For Eu MOFs **4**, a similar q value as the one reported in the literature [39] was obtained, while for samples with Eu/Y MOFs **1**, **2**, and **3**, the q values also augment by increasing the Y contents, e.g. 17.0%, 17.5%, 18.7% and 19.3% for **4**, **1**, **2**, and **3**, respectively. The lower numbers of water molecules in the Eu/Y MOFs reflect the alterations of Eu^{3+} ions first coordination shell, which is in agreement with the results obtained from the R values. Meanwhile, the decrease of k_{nr} together with the increase of k_r in Eu/Y MOFs results in an increase of q values, suggesting that there is a more efficient intramolecular energy transfer process in Eu/Y MOFs than in Eu MOFs. This phenomenon can be explained by a concentration dilution model [30]. For Eu compound **4**, self-quenching of the luminescence often occurs, while in mixed Eu/Y compounds **1**, **2** and **3**, Y^{3+} ions reduce the concentration self-quenching effect of Eu^{3+} ions to some extent and subsequently luminescence efficiency is increased.

4. Conclusion

Singular Eu or Y and three mixed europium–yttrium MOFs with different Eu/Y ratios as metal centers were prepared by hydrothermal synthesis. Compared with europium MOFs, the mixed europium–yttrium organic frameworks have identical crystal structure, as shown by single-crystal X-ray diffraction and PXRD analyses. In the mixed europium–yttrium MOFs, the photoluminescence studies indicate that the Eu^{3+} ions have longer lifetime and higher quantum efficiency than those in Eu MOFs. The PL quantum yields of the mixed europium–yttrium MOFs increase around 3–14% due to the decrease of the concentration self-quenching effect of Eu^{3+} ions. It can be speculated that the Eu quantum efficiency can be further increased, if the Eu/Y ratio is optimized. The obtained results indicate that the luminescent properties can be effectively enhanced through adding inert *Ln* ion to the luminescent MOFs. This work also opens a new route to improving luminescence properties of other *Ln* MOFs materials.

Appendix. Supplementary material

Complete crystallographic data for the structure reported in this paper have been deposited in the CIF format with the Cambridge Crystallographic Data Center as supplementary publication no. CCDC 830906, 830905, 830904, 834876 and 830907. Copies of the data can be obtained free of charge on application to CCDC, 12 Union Road, Cambridge CB2 1EZ, UK (fax: (44) 1223336-033; e-mail: deposit@ccdc.cam.ac.uk).

Acknowledgments

Y.F. Han is grateful to the financial support from FCT with the references of SFRH/BPD/63185/2009 and PTDC/CTM/108975/2008; F.-N. SHI and L.S. Fu acknowledge FCT for Ciência 2007 program.

Appendix A. Supporting materials

Supplementary data associated with this article can be found in the online version at doi:10.1016/j.jssc.2011.12.007.

References

[1] L.R. MacGillivray, Metal-organic Frameworks: Design and Application, John Wiley & Sons, 2010.
[2] G. Férey, C. Serre, T. Devic, G. Maurin, H. Jobic, P.L. Llewellyn, G. De Weireld, A. Vimont, M. Daturif, J.S. Chang, Chem. Soc. Rev. 40 (2011) 550–562.
[3] S.L. Qiu, G.S. Zhu, Coord. Chem. Rev. 253 (2009) 2891–2911.
[4] H.X. Deng, C.J. Doonan, H. Furukawa, R.B. Ferreira, J. Towne, C.B. Knobler, B. Wang, O.M. Yaghi, Science 329 (2010) 424–428.
[5] J.B. Lin, J.P. Zhang, X.M. Chen, J. Am. Chem. Soc. 132 (2010) 6654–6656.
[6] X.Y. Wang, Z.M. Wang, S. Gao, Chem. Commun. (2008) 281–294.
[7] S. Bureekaew, H. Sato, R. Matsuda, Y. Kubota, R. Hirose, J. Kim, K. Kato, M. Takata, S. Kitagawa, Angew. Chem. Int. Ed. 49 (2010) 7660–7664.

[8] F.N. Shi, L. Cunha-Silva, R.A.S. Ferreira, L. Mafra, T. Trindade, L.D. Carlos, F.A. Almeida Paz, J. Rocha, J. Am. Chem. Soc. 130 (2008) 150–167.
[9] Y.G. Huang, F.L. Jiang, M.C. Hong, Coord. Chem. Rev. 253 (2009) 2814–2834.
[10] K.A. White, S. Petoud, N.L. Rosi, Chem. Commun. (2009) 4506–4508.
[11] N. Kerbellec, D. Kustaryono, V. Haquin, M. Etienne, C. Daiguebonne, O. Guillou, Inorg. Chem. 48 (2009) 2837–2843.
[12] J. Rocha, L.D. Carlos, F.A.A. Paz, D. Ananiasa, Chem. Soc. Rev. 40 (2011) 926–940.
[13] C. Serre, F. Millange, C. Thouvenot, N. Gardant, F. Pellé, G. Férey, J. Mater. Chem. 14 (2004) 1540–1543.
[14] M.D. Allendorf, C.A. Bauer, R.K. Bhakta, R.J.T. Houk, Chem. Soc. Rev. 38 (2009) 1330–1352.
[15] P. Wang, J.-P. Ma, Y.-B. Dong, R.-Q. Huang, J. Am. Chem. Soc. 129 (2007) 10620–10621.
[16] X. Guo, G. Zhu, Q. Fang, M. Xue, G. Tian, J. Sun, X. Li, S. Qiu, Inorg. Chem. 44 (2005) 3850–3855.
[17] G.L. Law, K.L. Wong, Y.Y. Yang, Q.Y. Yi, G. Jia, W.T. Wong, P.A. Tanner, Inorg. Chem. 46 (2007) 9754–9759.
[18] K.A. White, D.A. Chengelis, K.A. Gogick, J. Stehman, N.L. Rosi, S. Petoud, J. Am. Chem. Soc. 131 (2009) 18069–18071.
[19] B.L. Chen, L.B. Wang, F. Zapata, G.D. Qian, E.B. Lobkovsky, J. Am. Chem. Soc. 130 (2008) 6718–6719.
[20] K. Liu, H.P. You, Y.H. Zheng, G. Jia, Y.H. Song, Y.J. Huang, M. Yang, J.J. Jia, N. Guo, H.J. Zhang, J. Mater. Chem. 20 (2010) 3272–3279.
[21] Y. Kim, M. Suh, D.-Y. Jung, Inorg. Chem. 43 (2004) 245–250.
[22] B.S. Zheng, J.F. Bai, J.G. Duan, L. Woitas, M.J. Zaworotko, J. Am. Chem. Soc. 133 (2011) 748–751.
[23] Y.F. Han, X.Y. Li, L.Q. Li, C.L. Ma, Z. Shen, Y. Song, X.Z. You, Inorg. Chem. 49 (2010) 10781–10787.
[24] M.D. Allendorf, C.A. Bauer, R.K. Bhakta, R.J.T. Houka, Chem. Soc. Rev. 38 (2009) 1330–1352.
[25] X. Peng, M.C. Schlamp, A.V. Kadavanich, A.P. Alivisatos, J. Am. Chem. Soc. 119 (1997) 7019–7029.
[26] Y.W. Cao, U. Banin, J. Am. Chem. Soc. 122 (2000) 9692–9702.
[27] D. Casanova, D. Giaume, T. Gacoin, J.-P. Boilot, A. Alexandrou, J. Phys. Chem. B 110 (2006) 19264–19270.
[28] C.R. De Silva, S. Smith, I. Shim, J. Pyun, T. Gutu, J. Jiao, Z.P. Zheng, J. Am. Chem. Soc. 131 (2009) 6336–6337.
[29] H.L. Guo, Y.Z. Zhu, S.L. Qiu, J.A. Lercher, H.J. Zhang, Adv. Mater. 22 (2010) 4190–4192.
[30] C.L. Choi, Y.F. Yen, H.H.Y. Sung, A.W.H. Siu, S.T. Jayarathne, K.S. Wong, I.D. Williams, J. Mater. Chem. 21 (2011) 8547–8549.
[31] D.T. de Lill, A. de Bettencourt-Dias, C.L. Cahill, Inorg. Chem. 46 (2007) 3960–3965.
[32] S. Surblé, C. Serre, F. Millange, F. Pelle, G. Férey, Solid State Sci. 7 (2005) 1074–1082.
[33] P. Mahata, K.V. Ramya, S. Natarajan, Dalton Trans. (2007) 4017–4026.
[34] K.M.L. Taylor, A. Jin, W.B. Lin, Angew. Chem. Int. Ed. 47 (2008) 7722–7725.
[35] S.M. Humphrey, R.A. Mole, R.I. Thompson, P.T. Wood, Inorg. Chem. 49 (2010) 3441–3448.
[36] E. Yang, J. Zhang, Z.J. Li, S. Gao, Y. Kang, Y.B. Chen, Y.H. Wen, Y.G. Yao, Inorg. Chem. 43 (2004) 6525–6527.
[37] X.Y. Tang, S.T. Yue, P. Li, N. Wang, Y.L. Liu, J. Rare Earths 26 (2008) 800–803.
[38] S.Y.C. Stephen, S. Alvin, F. Xue, Y.Z. Ze, C.W.M. Thomas, D.W. Ian, Inorg. Chem. Commun. 4 (2001) 467–470.
[39] M.O. Rodrigues, F.A.A. Paz, R.O. Freire, G.F. de Sá, A. Galembeck, M.C.B.S.M. Montenegro, A.N. Araújo, S. Alves, J. Phys. Chem. B 113 (2009) 12181–12188.
[40] APEX2, Data Collection Software Version 2.1-RC13, Bruker AXS, Delft, The Netherlands, 2006.
[41] Cryopad, Remote Monitoring and Control, Version 1.451, Oxford Cryosystems, Oxford, United Kingdom, 2006.
[42] SAINT+, Data Integration Engine Version 7.23a, Bruker AXS, Madison, WI, USA, 1997–2005.
[43] G.M. Sheldrick, SADABS Version 2.01, Bruker/Siemens Area Detector Absorption Correction Program 1998, Bruker AXS, Madison, WI, USA.
[44] G.M. Sheldrick, SHELXS-97, Program for Crystal Structure Solution, University of Göttingen, 1997.
[45] G.M. Sheldrick, SHELXL-97, Program for Crystal Structure Refinement, University of Göttingen, 1997.
[46] A.F. Kirby, D. Foster, F.S. Richardson, Chem. Phys. Lett. 95 (1983) 507–512.
[47] L.D. Carlos, Y. Messaddeq, H.F. Brito, R.A.S. Ferreira, V. de Zea Bermudez, S.J.L. Ribeiro, Adv. Mater. 12 (2000) 594–598.
[48] R.M. Supkowski, W.D. Horrocks, Inorg. Chim. Acta 340 (2002) 44–48.